# Experimental and Theoretical Investigations of the Ultrafast Photoinduced Decomposition of Organic Peroxides in Solution: Formation and Decarboxylation of Benzoyloxy Radicals

**Bernd Abel, Jens Assmann, Peter Botschwina, Michael Buback, Matthias Kling,* Rainer Oswald, Stefan Schmatz, Jörg Schroeder, and Thomas Witte**

*Institut für Physikalische Chemie, Universität Göttingen, Tammannstrasse 6, 37077 Göttingen, Germany*

*Received: April 2, 2003*

The light-induced (266 nm) ultrafast decarboxylation of two peroxides $R_1-C(O)O-OR_2$, with $R_1$ = phenyl and $R_2$ = benzoyl or *tert*-butyl, in solution has been studied on the picosecond time scale by absorption spectroscopy with a time resolution typically of 100 to 200 fs. The reaction was investigated in various solvents of different polarity and viscosity to elucidate the influence of the solvent environment on the decarboxylation rate. Transient intermediate benzoyloxy radicals, $R_1-CO_2$, were monitored at wavelengths between 300 and 1000 nm. While the primary dissociation of the peroxide is too fast to be resolved, the dissociation of intermediate benzoyloxy radicals is clearly detected on the picosecond time scale. The mechanism of light-induced two-step dissociation is discussed, as is the dependence of reaction dynamics on the type of substituent $R_2$ as well as the branching ratio between prompt and delayed $CO_2$ formation. A model for the decarboxylation process is presented that is based on molecular structure parameters and energies. The latter quantities, which are obtained from density functional theory calculations, serve as input data for calculations of the specific decomposition rate coefficients of benzoyloxy intermediates via statistical unimolecular rate theory. The predicted benzoyloxy radical decay data are compared with corresponding experimental concentration versus time traces.

## I. Introduction

Chemical reactions have been studied with continuously improving time resolution, which is accompanied by an improved understanding of elementary reaction mechanisms. Kinetics that appear to be straightforward with isolated molecules[1,2] become more difficult in solution because of complex interactions of reacting species with the molecular environment.[3] Nevertheless, bond fission,[4−10] structural isomerization,[11,12] intramolecular rearrangements,[13,14] solvation,[15,16] inter- and intramolecular energy transfer,[17−29] and internal conversion[16,30] as well as electron[30−32] and proton transfer[33−35] processes have recently been studied in the condensed phase by employing time-resolved femtosecond (fs) spectroscopy.

Complex light-induced reactions in solution can often be decomposed into a series of elementary reaction steps. Unimolecular rate theory should be helpful in rationalizing such individual processes.[36] The light-induced decarboxylation of organic peroxides with the general structure $R_1C(O)OOR_2$ is assumed to occur as a two-step unimolecular dissociation yielding two radicals and $CO_2$.[8] In Scheme 1, the decarboxylation of two such peroxides ($R_1$ = phenyl and $R_2$ = alkyl or benzoyl) is displayed schematically. In the first dissociation step, an aroyloxy and an alkoxy or two benzoyloxy radicals are formed by single-bond cleavage. In the subsequent dissociation step, the aroyloxy radicals decarboxylate to yield $CO_2$ and a phenyl radical. A sequential dissociation mechanism via short-lived intermediate aroyloxy radicals is favored over concerted bond scission leading directly to carbon dioxide because of the different bonds and bond energies involved.[37]

**SCHEME 1: Scheme of Sequential Dissociation after the Photoinduced Decomposition (266 nm) of Peroxides Investigated in the Present Study**

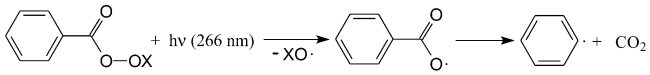


X = *tert*-butyl **(TBPB)** X = **(DBPO)**

Large organic peroxides belong to a group of molecules of fundamental as well as practical importance. They are widely used as initiators in free-radical polymerization.[38−40] Investigations on initiator dissociation mechanisms to answer the question of whether $CO_2$ formation occurs promptly or with some time delay are of eminent importance. The kinetics of such processes determines the time evolution of different types of intermediate radicals, carbon-centered or oxygen-centered, which in turn strongly affects the initiatior efficiency for free-radical polymerization.[8,41] A large body of literature exists on thermally induced peroxide decomposition.[39,41] Until recently, photochemically induced peroxide decompositions have mostly been investigated with nanosecond and microsecond time resolution using flash photolysis in conjunction with visible absorption or with EPR spectroscopy.[42−49] Although providing insight into the principal reaction channels and into some structural aspects of peroxide decomposition, such studies could not reveal mechanistic details of the photodissociation dynamics.[44,50] Obviously, further progress in this area requires investigations with subnanosecond time resolution. This need has been seen for quite some time, but in most cases, the required time resolution was not reached.[6−8,44,50−52] Moreover, insufficient

* Corresponding author. E-mail: mkling@gwdg.de.

10.1021/jp034858x CCC: $25.00 
Published on Web 06/06/2003

spectral resolution and spectral overlap prevented detailed studies. Whereas short-lived species could be detected in early picosecond studies,[51,52] the formation of $CO_2$ and its vibrational cooling in solution has been monitored on the picosecond time scale only recently via IR spectroscopy.[6−8] These studies revealed that peroxides decompose on an even shorter time scale. A recent femtosecond study on carbonyloxy radical intermediate decarboxylation was reported by Bockman et al.[53] However, the extended set of experimental data on thermal as well as on photochemical peroxide decomposition did not establish a (semi-)quantitative model that allows for a full understanding of existing data and the prediction of dissociation dynamics. In particular, the dependence of the dynamics on molecular structure, on internal energy, and on the solvent environment is not adequately understood.[8,41]

The decarboxylation, for example, of peroxyesters in solution, is accompanied by competing processes such as intermolecular vibrational energy transfer (VET)[17,19,20,29,54] and may be obscured by spectral congestion of parent molecules, intermediates, and products.[42,48,49] A full interpretation of experimental observables on the molecular level requires ultrafast absorption spectroscopy with sufficient time and spectral resolution over extended ranges of probe wavelengths. The spectra of intermediates and products should be known, and quantum chemical methods should be applied to map out the molecular structures and energetics as well as the relevant features of the potential energy surfaces (PES) on which the reactions proceed. In addition, the time evolution of intermediates and products should be recorded with more than one experimental technique (e.g., using absorption spectroscopy in the visible, near-infrared, and infrared ranges).

In the present article, we report studies on the decomposition process of *tert*-butyl peroxybenzoate (TBPB) and dibenzoyl peroxide (DBPO) in solution. A special feature of our approach is that femtosecond absorption spectroscopy experiments are carried out in conjunction with density functional theory calculations and theoretical modeling of the observables. The two classical peroxides are easily excited by UV light at 266 nm because of their aromatic chromophore. The thermal decomposition and decarboxylation of these peroxides have been extensively studied in the past.[41] An overview of thermally induced decomposition experiments and of time-resolved studies with nanosecond time resolution is given in refs 8 and 44.

Our paper is organized as follows: After a brief description of the experimental procedure, the static and transient spectra of intermediates and products are discussed. These spectra allow for the selection of spectral regions where intermediates and products may be quantitatively observed without significant spectral congestion, overlap, and interference. The measured time-resolved spectral traces will be presented, as will the results of density functional theory (DFT) calculations that yield the structures and energies of intermediates and transition states (minima and first-order saddle points) to be used as input parameters for the calculation of statistical specific rate constants. Finally, we propose a semiquantitative model for the decarboxylation of aroyloxy radicals that is based upon quantum chemical calculations and statistical unimolecular rate theory, which allows us to model the experimental concentration versus time profiles satisfactorily.

## II. Experimental Section

The Ti:sapphire laser system (Verdi, Coherent, ORC1000, Clark) with regenerative amplifier (RGA), described in more detail elsewhere,[55] generates 40-fs pulses (800 nm, 0.7 mJ/pulse) at a 1-kHz repetition rate. The laser pulses were split into two parts: 30% of the pulse energy was used for second- and third-harmonic generation (SHG, THG) in two nonlinear crystals (BBO) and finally for peroxide excitation at 266 nm. The second part of the RGA output (70%) was used to pump an optical parametric amplifier (TOPAS, Light Conversion). The TOPAS output was frequency mixed to provide a probing wavelength in the range from 300 to 1000 nm. The delay between the pump and probe pulses was set with a computer-controlled translation stage (Newport). The two laser pulses were mildly focused ($f = 200$ mm) and overlapped in time in a fast-flow cell (0.1−0.2 mm thickness). Pulses with relative polarization at the magic angle (54.7°) in a nearly collinear pump/probe geometry (5°) were chosen for the present experiments. Transient difference absorbance was recorded at a 1-kHz repetition rate before and behind the cell (containing the peroxide solution having an optical density close to OD = 2 at the pump wavelength). For active background subtraction, the data were taken on alternating shots with and without pump pulses. Time-resolved transients were recorded at various probe wavelengths averaging up to 8000 pulses at each wavelength. Experiments were partially carried out with another setup[56] consisting of a Ti:sapphire regenerative amplifier (CPA-2001, Clark-MXR) and two optical parametric amplifiers (TOPAS, Light Conversion and NOPA, Clark-MXR). Although probe pulses in the same wavelength range have been provided by the TOPAS, tunable pump pulses (230−350 nm) were obtained by second-harmonic generation of the NOPA signal. Typical time resolutions of 100−200 fs were obtained in solution. No difference in the experimental curves is seen between data from the two laser setups. All high-purity grade peroxides were synthesized and kindly provided by AKZO Nobel (Research Center Deventer, The Netherlands). Solvents of the highest quality were purchased from Merck. Peroxides and solvents have been used without further purification.

## III. Results and Discussion

**A. UV/Vis Spectra of Parent Molecules, Intermediates, and Products.** The static and transient spectra of the parent molecules, intermediates, and products will be discussed first. A commercial Varian CARY 5E spectrometer has been used to measure the static UV absorption spectra of the peroxides in propylene carbonate (PC) solution. (The spectra are given in the Supporting Information.) The diffuse absorption bands of DBPO and TBPB between 260 and 290 nm may be assigned to the characteristic $\pi^* \leftarrow$ n transition of the carbonyl group.[57] Excitation into the repulsive electronic state results in ultrafast direct dissociation.[58] According to Scheme 1, primary dissociation of the peroxides generates two benzoyloxy radicals (with DBPO) or a benzoyloxy and an alkyloxy radical (with TBPB). The benzoyloxy radicals subsequently decompose into phenyl radicals and $CO_2$.

In solution, the benzoyloxy radical exhibits a characteristic broad absorption band in the visible region from about 450 to beyond 800 nm and a sharper absorption component with a maximum at around 400 nm. The spectrum was measured by Misawa et al. in a flash photolysis experiment.[48] Ingold et al. attributed the visible absorption above 450 nm to a transition from the $^2B_2$ electronic ground state to the second excited ($^2A_1$) state.[42,49] Although there is agreement about the assignment of the transition $^2A_1 \leftarrow$ ground state, there is still some debate as to whether the $^2A_2$ or the $^2B_2$ state is lower in energy and thus constitutes the electronic ground state.[49,59−61] The approximate energy difference to the $^2A_1$ state may be determined from the

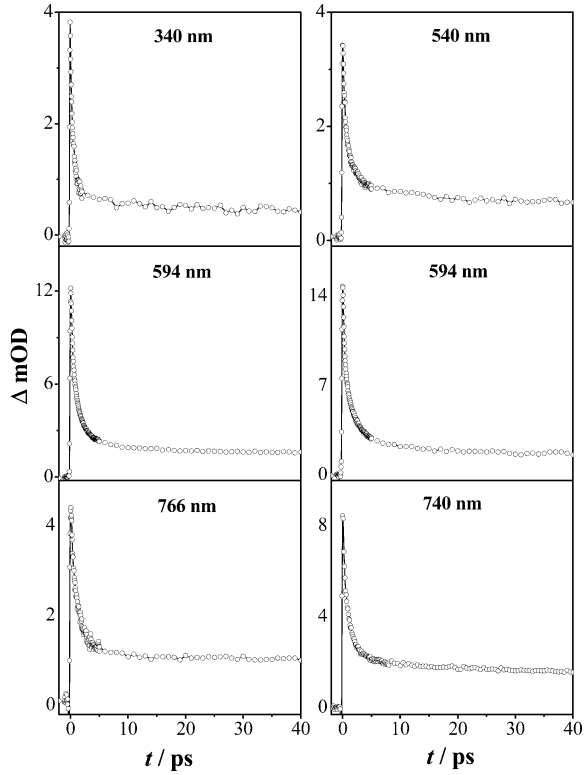


**Figure 1.** Time-resolved difference absorption, ΔOD, of benzoyloxy radicals in the decomposition studies on TBPB (left column) and DBPO (right column) in propylene carbonate after excitation at 266 nm.

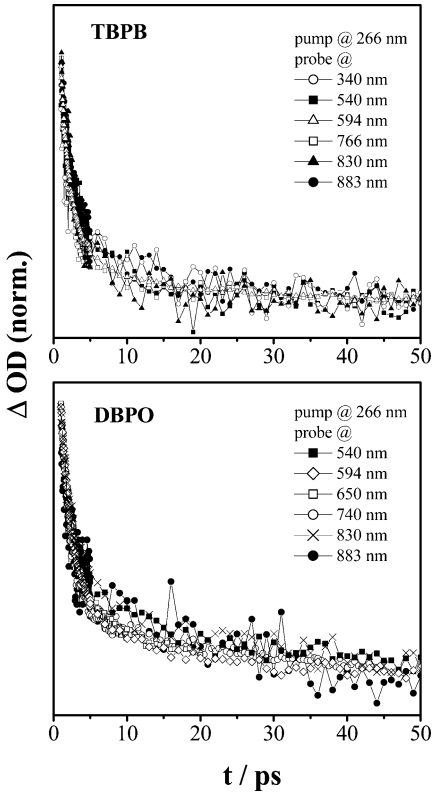


**Figure 2.** Time-resolved difference absorption, ΔOD, of benzoyloxy radicals from the decomposition of TBPB and DBPO measured at several wavelengths after 266-nm excitation. Curves are superimposed.

maximum of the spectrum, which is located at around 800 nm (corresponding to 12 500 $cm^{-1}$).[44,48] As will be shown later, the energy of this state is important for the contribution of the direct (immediate) dissociation of benzoyloxy radicals.

The phenyl radical has a well-known strong absorption in the UV spectral range with a maximum at 240 nm.[62] The absorbance of the phenyl radical was determined by gas-phase studies[62,63] and was found to be too low to overlap the absorption of the benzoyloxy radical significantly at wavelengths above 330 nm.[48] Phenyl radicals, in addition, show an optical transition between 440 and 530 nm[62] that is even weaker and thus did not contribute to the overall transient absorption in previous nanosecond studies on TBPB and DBPO decomposition.[48,49] Also, the alkoxy radicals, produced from TBPB, do not show any significant absorption in the near-UV and visible spectral ranges.

**B. Decarboxylation Measured with Femtosecond Pump and Probe Spectroscopy.** The stepwise photoinduced decarboxylation of organic peroxides in solution may be followed by probing intermediate radicals or products via time-resolved absorption spectroscopy. The formation of $CO_2$ and its vibrational cooling, the latter of which manifests itself in a narrowing and shifting of the transient IR spectra of the $\nu_3$ mode, can be monitored by transient IR spectroscopy at around 4.3 $\mu$m.[6−8] In the present study, we monitor the intermediate benzoyloxy radical via femtosecond visible absorption spectroscopy.

After the photolysis of *tert*-butyl peroxybenzoate (TBPB) in PC at 266 nm, time-resolved transients for the intermediate benzoyloxy radical were recorded at $\lambda_{probe}$ = 340, 540, 594, 766, 830, and 883 nm. Examples of the resulting optical density (OD) versus time traces are plotted in the left column of Figure 1. As a characteristic feature of all of these traces, an instantaneous rise and a subsequent decay in absorption are seen. The formation of benzoyloxy radicals from the photolysis of the parent peroxide occurs too rapidly to be resolved. The subsequent decarboxylation, however, may be easily followed on the picosecond time scale. The "offset" of optical density toward larger reaction times reflects the much slower thermal reaction of benzoyloxy radicals after energy relaxation.

Intense absorption up to about 300 fs may be affected by nonlinear effects of the interaction of pump and probe pulses with the medium. However, at delay times beyond 500 fs, the signals can exclusively be attributed to the absorption of benzoyloxy radicals. This species has already been investigated with nanosecond time resolution.[44,46,48,49]

Transient absorption traces of dibenzoyl peroxide (DBPO) in propylene carbonate solution following excitation at 266 nm were recorded at $\lambda_{probe}$ = 540, 594, 650, 740, 830, and 883 nm. A representative set of these traces reflecting the time dependence of the benzoyloxy radical concentration is shown in the right column of Figure 1. Again, as with TBPB, the individual traces, besides some differences in amplitude modulation, display the same temporal behavior for all wavelengths throughout the region from 540 to 883 nm.

To illustrate that the experimental traces recorded at different wavelengths above 300 nm represent the same kinetics, normalized traces (obtained after the subtraction of the offset and amplitude scaling) are plotted for probe wavelengths between 300 and 900 nm (Figure 2). No significant change with probe wavelength is found in this spectral region, indicating the exclusive observation of the benzoyloxy radical.

This might not be the case for each solvent, especially for smaller polar solvent molecules (e.g., acetonitrile), which can be subject to solvation around the COO moiety of the benzoyloxy radical. In such cases or when significant spectral narrowing due to the cooling of benzoyloxy radicals takes place, the benzoyloxy radical spectrum may show a temporal evolution overlapping the decarboxylation dynamics. However, by re-

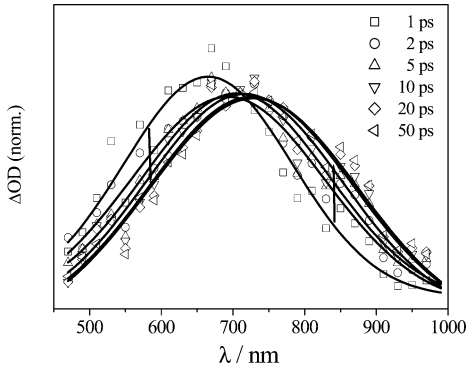


**Figure 3.** Transient spectra at various delay times reconstructed from single measurements of the difference absorption, ΔOD, of benzoyloxy radicals in the decarboxylation studies of DBPO (282-nm excitation in acetonitrile). The arrows indicate changes in the benzoyloxy radical spectrum with time.

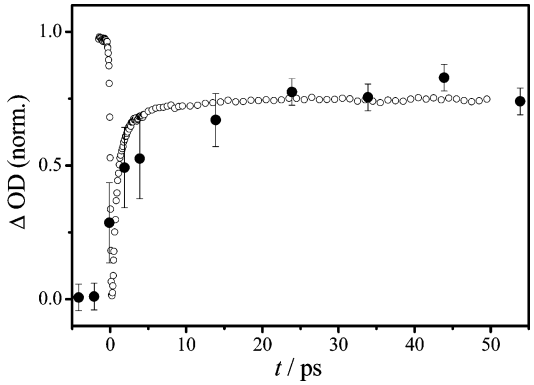


**Figure 4.** Absorbance change due to the decay of the benzoyloxy radical concentration and the formation of $CO_2$ deduced from different experiments. (○) Normalized and inverted transient absorption of benzoyloxy radicals measured during the photoinduced (266 nm) decomposition of DBPO in dichloromethane at 700 nm. (●) $CO_2$ product absorbance deduced from integrated transient absorption at 4.3 $\mu$m during photolysis (248.5 nm, ref 8).

constructing the benzoyloxy radical spectrum for several delay times after the photoinduced decomposition of a particular peroxide, ideal observation points for the exclusive observation of the benzoyloxy radical decarboxylation can be identified. Figure 3 shows reconstructed normalized spectra from single ΔOD versus time profiles at wavelength between 470 and 970 nm measured after the photolysis of DBPO at 282 nm. Regardless of the poor signal-to-noise ratio of the reconstructed spectra, some key features can be seen:

The benzoyloxy radical spectrum shows a noticeable red shift in time with a time constant of a few picoseconds. However, the overall spectral changes are not very pronounced. At around 700 nm, the spectral evolution with time is the smallest.

The spectral evolution with time is assumed to originate mainly from a combination of the cooling of hot benzoyloxy radicals and solvation. These two processes cannot be clearly identified and distinguished from each other, thus making the determination of individual time constants unfeasible. However, besides a larger evolution of the spectrum within the first 2 ps, the differences between spectra at longer delay times are small, limiting the time constants of processes responsible for spectral evolution to a few picoseconds. Unperturbed observation of benzoyloxy radical concentration versus time profiles is possible at around 700 nm, where no significant change in spectral intensity with time is seen. Reconstructing the temporal evolution of benzoyloxy radical spectra helps in identifying ideal observation points for a particular solvent.

The maximum of the benzoyloxy radical spectrum detected after the UV photolysis of DBPO in acetonitrile was reported to be around 800 nm.[48,49] Taking into account the signal-to-noise ratio of spectra given in the literature[48,49] and the spectra presented in Figure 3, we determined the location of the maximum to be between 750 and 800 nm, in good agreement with our theoretical calculations for the $^2B_2$ ground to $^2A_1$ excited-state vertical transition as described in section IIIC.

It appears desirable to monitor, in addition to the kinetics of the benzoyloxy radical, the generation and energy of the products (i.e., the phenyl radical and $CO_2$) with femtosecond time resolution. Although the phenyl radical could not be detected because of overlapping parent molecule absorptions, the formation of $CO_2$ was monitored by the rise of the integral absorbance of the asymmetric stretching band in the IR over the range from 2200 to 2450 $cm^{-1}$.[8]

In Figure 4 , the change in optical density due to benzoyloxy radical concentration monitored at 700 nm after the photodissociation of DBPO at 266 nm in dichloromethane is compared with the time evolution of $CO_2$ after the excitation of DBPO at 248.5 nm in the same solvent. The latter curve is affected by larger errors within the first 10 to 15 ps that are due to solvent signal subtraction, leading to an effective time resolution of the IR experiment of a few picoseconds.[8] Nevertheless, the close agreement of the temporal behavior of these two species obtained from complementary experiments supports our assumption that we exclusively observe the decarboxylation process of benzoyloxy radicals.

**C. Quantum Chemical Calculations.** The calculations of geometries and energies were performed for isolated molecules (i.e., molecules in the gas phase). The results should be applicable to situations where the molecules are embedded in an environment of nonpolar and perhaps even of weakly polar aprotic solvent molecules as employed in our spectroscopic experiments. According to earlier experimental and theoretical work,[59,64] the electronic ground state of the benzoyloxy radical is of $^2B_2$ symmetry and exhibits a planar equilibrium structure. In this work, geometry optimizations were carried out with the density functional theory (DFT) variant UB3LYP[65,66] in conjunction with the 6-31G(d) and 6-311+G(d,p) basis sets. For benzoyloxy, these comprise 145 and 228 contracted Gaussian-type orbitals (cGTOs), respectively. Gaussian98[67] was used in all of the DFT calculations reported in this work.

The structures of the relevant stationary points (reactant, products, and first-order saddle points corresponding to decarboxylation and rotation around the C−$CO_2$ bond, respectively) on the potential energy surface (PES) of the benzoyloxy radical were fully optimized at the UB3LYP level of theory. To confirm that true minima on the PES have been found, the Hessian matrices at the stationary points were calculated. The energies were further corrected for zero-point vibrational effects (at the harmonic level; imaginary frequencies not included). The TS routine of Gaussian98 and the intrinsic reaction coordinate (IRC) method[68,69] were employed for the calculation of the transition-state (first-order saddle point) geometries.

At the geometries of the stationary points, single-point calculations with the 6-311+G(2d,p) and 6-311+G(2df,2pd) basis sets, which for benzoyloxy comprise 273 and 376 cGTOs, respectively, were carried out (Table 1). As is commonly observed for DFT methods, changes due to basis saturation effects are only of minor importance. Because the basis set limit is reached faster in density functional theory than in conventional wave function-based methods, the error due to basis set truncation (basis set superposition error, BSSE) is estimated to be very small.

**TABLE 1: Relative Energies of Reactants and Transition States (kcal mol$^{-1}$) for Decarboxylation ($PhCO_2 \rightarrow Ph + CO_2$) and Internal $CO_2$ Rotation[a]**

| Ph−$CO_2$ | method | basis set | $E_{el}$ | $E_0$ | $\Delta_r H^\circ$ (298 K) |
|---|---|---|---|---|---|
| decarboxylation barrier height | UB3LYP | 6-31G(d) | 12.30 | 10.67[c] | |
| | | 6-311+G(2d,p)[b] | 10.76 | 9.13[c] | |
| | | 6-311+G(2df,2pd)[b] | 9.51 | 7.87[c] | |
| | | 6-311+G(d,p) | 10.05 | 8.54[e] | |
| | | 6-311+G(2d,p)[d] | 10.82 | 9.32[e] | |
| | | 6-311+G(2df,2pd)[d] | 9.94 | 8.43[e] | |
| | UB3PW91 | 6-31G(d) | 12.41 | 10.83[c] | |
| | | 6-311+G(2d,p)[b] | 10.70 | 9.12[c] | |
| | | 6-311+G(2df,2pd)[b] | 9.84 | 8.26[c] | |
| | | 6-311+G(d,p) | 10.16 | 8.68[e] | |
| | | 6-311+G(2d,p)[d] | 10.74 | 9.26[e] | |
| | | 6-311+G(2df,2pd)[d] | 9.91 | 8.43[e] | |
| $CO_2$ rotation barrier height | UB3LYP | 6-31G(d) | 5.87 | 5.32[c] | |
| | | 6-311+G(2d,p)[b] | 3.95 | 3.40[c] | |
| | | 6-311+G(2df,2pd)[b] | 3.68 | 3.13[c] | |
| | | 6-311+G(d,p) | 4.08 | 3.58[e] | |
| | | 6-311+G(2d,p)[d] | 3.93 | 3.43[e] | |
| | | 6-311+G(2df,2pd)[d] | 3.95 | 3.45[e] | |
| | UB3PW91 | 6-31G(d) | 5.78 | 5.30[c] | |
| | | 6-311+G(2d,p)[b] | 4.09 | 3.61[c] | |
| | | 6-311+G(2df,2pd)[b] | 4.13 | 3.65[c] | |
| | | 6-311+G(d,p) | 4.27 | 3.77[e] | |
| | | 6-311+G(2d,p)[d] | 4.11 | 3.61[e] | |
| | | 6-311+G(2df,2pd)[d] | 4.15 | 3.65[e] | |
| decarboxylation | UB3LYP | 6-311+G(2df,2pd)[b] | −0.51 | | −1.76[f] |
| | UB3PW91 | 6-311+G(2df,2pd)[b] | 0.36 | | −0.83[f] |
| | RCCSD(T) | 347 cGTOs (see text) | 0.50 | | −0.69[g] |

[a] The energy of the reactant is set to zero for all methods and basis sets used in the calculations. Reaction enthalpies for decarboxylation are also given in kcal mol$^{-1}$. $E_{el}$ denotes the electronic energies including nuclear repulsion, and $E_0$ additionally includes corrections due to zero-point vibrational effects (harmonic level). Absolute energy values in hartrees are available upon request. [b] Calculated using the 6-31G(d) geometries. [c] ZPE calculated employing the 6-31G(d) basis set. [d] Calculated using the 6-311+G(d,p) geometries. [e] ZPE calculated employing the 6-311+G(d,p) basis set. [f] ZPE and thermal corrections for 298 K calculated with the 6-31G(d) basis set. [g] ZPE and thermal corrections for 298 K calculated with the UB3LYP method and the 6-31G(d) basis set.

Under the assumption of $C_{2v}$ symmetry and taking the geometrical parameters of the phenyl moiety from the UB3LYP calculations with the 6-31G(d) basis, large-scale coupled cluster calculations were employed in an optimization of the remaining three geometrical parameters $r_1$(C−C), $r_2$(C−O), and α(OCO). These made use of partially restricted coupled cluster theory based on a restricted Hartree−Fock determinant as formulated by Knowles et al.[70] and integrated into the MOLPRO[71] suite of programs. The version that was employed is RCCSD(T), which includes connected triple substitutions by means of perturbation theory. A flexible basis set of 347 cGTOs was used in these calculations. For the carbon and hydrogen atoms, Dunning's cc-pVTZ basis[72] was employed, with d functions left off at the hydrogen atoms. For the oxygen atoms, the corresponding augmented basis set aug-cc-pVTZ[73] was employed.

The optimum geometrical parameters obtained by RCCSD(T) are $r_{1e} = 1.4715$ Å, $r_{2e} = 1.2649$ Å, and $\alpha_e = 110.63°$. According to our experience with comparable calculations for well-known molecules, the two equilibrium bond lengths are overestimated by about 0.007 Å. These errors mainly result from the neglect of core−valence correlation and the use of an incomplete basis set. The geometrical parameters obtained by UB3LYP/6-311+G(d,p) are 1.472 Å, 1.266 Å, and 111.9° and are thus rather close to the above RCCSD(T) values.

At the mixed UB3LYP/RCCSD(T) equilibrium structure, the electric dipole moment of the $^2B_2$ state is calculated to be 4.26 D (RCCSD(T)/347 cGTOs), with the negative end of the dipole at the site of the oxygen atoms. The corresponding value for the phenyl radical is 0.850 D. The rather high value for the benzoyloxy radical results from significant charge transfer to the bent $CO_2$ moiety.

We have used RCCSD(T)/347 cGTOs to calculate vertical transition energies to three singly excited electronic states of different symmetry. In order of energy, these are of $^2A_2$, $^2A_1$, and $^2B_1$ symmetry. From the ground state, the transition to the $^2B_1$ state is electronically forbidden. Calculated vertical transition energies (in cm$^{-1}$) are 6276, 12 943, and 21 075. The second value, which corresponds to a wavelength of 773 nm, correlates well with the observed absorption band (cf. section III.A). Because of its rather high excitation energy, the $^2B_1$ state is not expected to play a role in the present experiments. From a theoretical point of view, the situation in that energy range may be much more complicated, anyway.

As was described by Pacansky and Brown,[74] it is only the $^2A_1$ state that correlates with the ground states of both the phenyl radical and the carbon dioxide molecule. For the decarboxylation process to occur, the breaking of a C−C $\sigma$ bond is crucial, leading to a $\sigma$-SOMO in the $^2A_1$ ground state of the phenyl radical. The benzoyloxy state that correlates with this product state must also have a $\sigma$-SOMO. Thus, the $^2A_2$ and $^2B_1$ states need not be considered in the thermal unimolecular reactions because their SOMOs exhibit $\pi$ character.

Upon vertical excitation from the ground state, a strongly repulsive region of the $^2A_1$ PES is reached. At the geometry of the $^2B_2$ ground state, the $^2A_1$ state has an electric dipole moment of 4.52 D, which is quite similar to that of the electronic ground

state. We may thus expect that solvation effects are not very different in this electronically excited state.

In $C_{2v}$ symmetry, the PESs of the $^2A_1$ and $^2B_2$ states may intersect. This conical intersection may play a crucial role in the nuclear dynamics. However, in the actual reaction process, $C_{2v}$ symmetry may not be very important for several reasons: First, the benzoyloxy radical produced by dissociation of the O−O bond in TBPB or DBPO is highly distorted from its equilibrium geometry. The asymmetric CO stretching vibration is excited, as is the hindered internal rotation around the Ph−$CO_2$ bond. Because the dissociation barrier is much higher than the barrier for internal rotation (see below), the $CO_2$ group can almost freely rotate at chemically relevant energies. Second, the reaction takes place in solution. The solvent molecules influence the molecular PES and at least perturb the symmetry. We thus assume that the reaction may well be described by a single PES (i.e., by the lower sheet of the two surfaces forming the conical intersection). In this adiabatic approximation, a saddle point appears instead of the double cone.

Our second assumption is that density functional theory without symmetry restrictions is capable of providing a reasonably good approximation of the PES in the saddle-point region. This assumption lacks a sound theoretical basis but appears to be reasonable and is corroborated by the following facts: First, the DFT calculations yield a physically reasonable saddle-point structure with an appropriate reactive normal coordinate. Second, in contrast to systems with several low-lying interacting electronic states, no convergence problems have been observed. Third, the barrier height employed in statistical rate-theory calculations yields very good agreement with experimental data.

Because of the flatness of the PES in the vicinity of the saddle point pertinent to decarboxylation, the search for this structure turned out to be relatively complicated for aryloxycarbonyloxy and benzylcarbonyloxy radicals.[75] In the case of the benzoyloxy radical, the search was less time-consuming because of the highly symmetric structure of the saddle-point geometry. However, $C_{2v}$ symmetry was not used in the calculations, but $C_1$ symmetry was adopted to account for the following situation: According to the first Hohenberg−Kohn theorem,[76] the Hamiltonian (i.e., the external potential) is uniquely defined by the electron density of the ground electronic state. Density functional calculations carried out in a particular molecular point group yield the energy of the lowest electronic state of this symmetry. Our approach is not restricted to spatial symmetry and may thus yield an appropriate description of the reaction coordinate from the reactant species ($^2B_2$) to the products ($^1A_1$ and $^1\Sigma_g^+$).

According to our UB3LYP/6-311+G(d,p) calculations, in the saddle-point species pertinent to decarboxylation, the Ph−$CO_2$ distance is elongated to 1.875 Å, and the $CO_2$ group is characterized by two C−O bonds of 1.199-Å length that include a bond angle of 149.1°. Thus, the C−O bonds are already considerably shortened, and the O−C−O angle has been enlarged by as much as 38°. The reactive normal coordinate, $Q_{TS}$ (Figure 5), describes the stretching of the Ph−$CO_2$ bond and the simultaneous widening of the O−C−O angle. Note that the displacement vector of the carbon atom in the $CO_2$ group dominates $Q_{TS}$.

A further stationary point on the benzoyloxy PES is of interest for a more complete description of reaction dynamics, viz., the first-order saddle point that corresponds to the rotation of the $CO_2$ unit around the Ph−$CO_2$ axis. This transition state structure at 3.45 kcal mol$^{-1}$ (UB3LYP/6-311+G(2df,2pd)//6-311+G(d,p), Table 1) exhibits $C_{2v}$ symmetry with the $CO_2$ plane perpendicular to the phenyl plane. It is located considerably below the barrier to dissociation so that it has to be anticipated that the hindered rotation around the Ph−$CO_2$ bond is possible at chemically relevant energies, thus easily breaking the $C_{2v}$ symmetry of the benzoyloxy radical in its equilibrium configuration. This saddle point has already been calculated with the B3PW91 functional at the 6-311+G(d,p) level of theory by Kieninger et al., who obtained a barrier height in agreement with the value given in Table 1.[64]

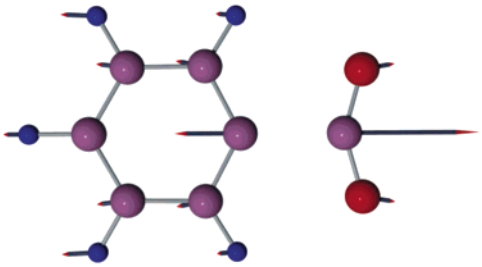

**Figure 5.** Representation of the normal mode with imaginary frequency (reaction coordinate, $Q_{TS}$) at the saddle point for the decarboxylation of the benzoyloxy radical. For details, see the text.

**TABLE 2: Harmonic Vibrational Frequencies of the Reactant (Ph−$CO_2$) and Saddle-Point Species (TS) (in cm$^{-1}$)[a]**

| Ph−$CO_2$ | TS |
|---|---|
| 45.0, 151.9, 179.9, 374.6, 405.8, 428.3, 502.5, 629.4, 642.9, 681.1, 703.4, 795.0, 798.8, 862.5, 955.2, 999.1, 1016.4, 1018.6, 1043.4, 1100.1, 1124.2, 1170.6, 1187.0, 1202.7, 1341.5, 1355.3, 1481.2, 1513.5, 1567.6, 1623.2, 1642.3, 3170.2, 3179.9, 3184.4, 3193.4, 3198.0 | 252.5*i* (reaction coordinate), 27.1, 131.5, 194.4, 250.0, 415.9, 434.7, 471.7, 606.1, 635.1, 657.9, 682.6, 749.8, 808.7, 927.3, 967.6, 983.9, 1002.8, 1019.6, 1050.0, 1081.5, 1179.2, 1183.4, 1246.6, 1310.1, 1324.4, 1464.6, 1478.4, 1580.1, 1621.3, 1945.0, 3168.9, 3177.1, 3191.8, 3223.5, 3224.2 |

[a] Results from UB3LYP/6-311+G(d,p) calculations.

Relative energies of reactants and of transition states as obtained in our UB3LYP calculations are summarized in Table 1, together with results obtained by employing the B3PW91 correlation functional of Perdew et al.[77,78] The differences between the data calculated with the two functionals appear to be negligible. The entries in Table 1 show that the benzoyloxy decarboxylation is almost thermoneutral, in accordance with the experimental observation reported by Jaffe et al. in 1957.[79] The thermoneutrality may be explained by the stabilization of both reactants and products by electron delocalization and/or aromaticity effects. In the benzoyloxy radical, the phenyl and $CO_2$ units allow for complete electron delocalization whereas the $CO_2$ and aromatic phenyl radical products are particularly stable species.

The harmonic vibrational frequencies $\omega_i$ that were calculated for the reactant and for the saddle-point geometries are reported in Table 2. These are important input data for the statistical rate-coefficient calculations described below.

**D. Model for the Sequential Decomposition of Peroxides.** The comprehensive treatment of chemical transformations in solution is still a big challenge.[80,81] Before turning to quantitative modeling, a few well-known aspects need to be addressed and summarized: (i) The absorption of 266-nm radiation excites the peroxide (DBPO or TBPB) into the repulsive $S_1$ state.[58,82] (ii) The concerted elimination of $CO_2$ by the simultaneous fission of two bonds is rather unlikely because of the very different chemical nature of the bonds; therefore, fast sequential

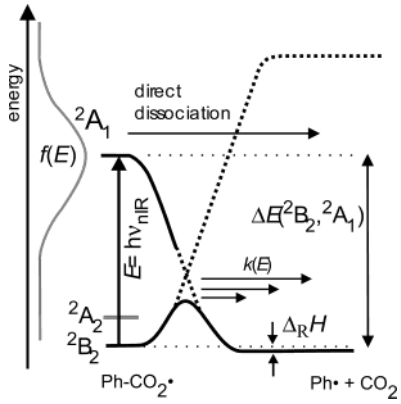


**Figure 6.** Schematic potential energy diagram with an illustration of the two decarboxylation pathways of excited benzoyloxy radicals. $f(E)$ is the vibrational energy distribution of the benzoyloxy radical, $k(E)$ denotes specific rate constants of the intermediate radical, $\Delta E$ is the energetic separation of the ground and second excited states of the benzoyloxy radical, and $\Delta_r H$ is the reaction enthalpy for the dissociation of the benzoyloxy radical to $CO_2$ and phenyl. For further details, see the text.

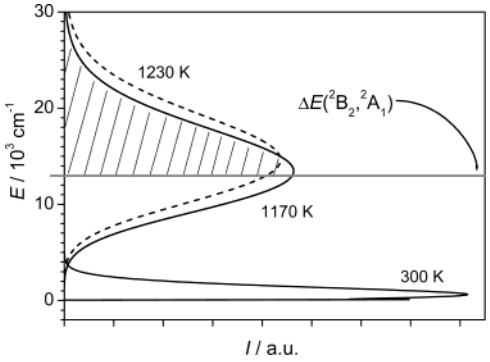


**Figure 7.** Representation of thermal energy distributions at 300 and 1170 K for the benzoyloxy radical after the dissociation of TBPB at 266 nm and the energetic location of the $^2A_1$ state (grey horizontal line). The energy distribution at 300 K was scaled by a factor of 0.25 for better comparison. Also shown is an energy distribution at 1230 K for the benzoyloxy radical after the dissociation of TBPB at 248.5 nm (dashed line).

dissociation is considered to be the rule rather than the exception for the decomposition of organic peroxides, even in solution.[35,37]

Beyond these established facts our model requires the following approximations, which are assumed to be justified in the present studies:

(1) The direct dissociation of DBPO and TBPB (approximately within one vibrational period) can produce vibrationally excited benzoyloxy radical(s) in the electronic ground $^2B_2$ state and in the second excited $^2A_1$ state.

(2) Because the second excited state,$^2A_1$, correlates with the ground state of the product radical,[74] the electronically excited intermediate may react in a fast, barrierless "downhill reaction" to produce vibrationally excited products (Figure 6). The coupling of the states in this energy region is assumed to be strong. With sufficient excess energy being available, this reaction channel will be the preferred one. This process releases vibrationally highly excited $CO_2$, which may be observed experimentally.[6−8]

(3) In applying our model, we implicitly assume that solvent polarity and viscosity have negligible effects on the dynamics of the reaction. The validity of this assumption will be shown by comparing dissociation dynamics measured in different solvents. The solvent turns out to act merely as a heat bath providing a sink for excess energy.

The location of the excited $^2A_1$ state of the benzoyloxy radical may be probed via the optical transition in the near-IR range[48,49] because it is actually the upper state in our probe transition[74] (Figure 6). Its location relative to the mean excess energy determines the branching ratio between the excited- and the ground-state channels whereas the barrier height determines average lifetimes and product state distributions of the fragments produced by the ground-state reaction (which is also schematically depicted in Figure 6). The latter reaction is monitored in our experiment.

Experimentally, we face the situation that both the dissociation of the parent peroxide as well as the direct dissociation from the electronically excited state of the intermediate radical are too fast to be resolved in time. The decarboxylation of the intermediate radical on the ground state PES is also fast but may be accurately measured. Assuming fast internal equilibration, this reaction may be treated by statistical unimolecular rate theory.[36] In applying our model, we make the additional assumption that in the initial dissociation of the parent peroxide the initial excess energy is statistically distributed among the two ground-state radical fragments (i.e., that a vibrational temperature may be assigned to intermediate radicals and products).

We have recently highlighted experiments on the decomposition of di(1-naphthoyl) peroxide.[56] 1-naphthoyloxy radicals have been identified as intermediates that dissociate without the involvement of electronically excited states. The electronically excited state, which is responsible for direct decarboxylation, turned out to be too high in energy as to be accessible after 266-nm excitation. Therefore, the reaction of intermediate radicals could be well described by a ground-state barrier reaction. For benzoyloxy radicals, the relevant electronically excited state appears to be sufficiently low-lying to be accessed in the 266-nm photodissociation of the parent peroxides.

This fast reaction from the electronically excited state rapidly depletes, on a subpicosecond time scale, the benzoyloxy radical population in the high-energy part of the energy distribution. The solvent is unable to repopulate the high-energy levels on the time scale of the reaction. Once the fast excited-state reaction has in this way depleted the high-energy tail of the energy distribution, the remaining radicals react in a statistical fashion on the ground-state PES over the barrier to products.

The mean value of the energy distribution of benzoyloxy radicals immediately after formation is calculated from the photon energy at $\lambda = 266$ nm and from the enthalpy of reaction for peroxide dissociation leading to benzoyloxy radicals. The enthalpy of reaction $\Delta_r H$ at 298 K was calculated to be 19.8 kcal mol$^{-1}$ for TBPB dissociation (B3LYP/6-311+G(2d,p)) and 19.2 kcal mol$^{-1}$ for DBPO dissociation (B3LYP/6-311+G(d,p)//6-31G(d,p)). The mean energy of intermediate radicals is estimated, assuming that the initial excess energy after photoexcitation of the peroxides at 266 nm is statistically distributed among the fragments of primary peroxide decomposition. In this way, initial mean energies for the benzoyloxy radical of 14 400 cm$^{-1}$ for TBPB and 13 500 cm$^{-1}$ for DBPO were determined.

The fraction of intermediate benzoyloxy radicals dissociating via the excited state is estimated via a simple energy-partitioning model taking into account the energy difference between the $^2A_1$ excited state and the $^2B_2$ ground state as well as the initial energy distribution of the benzoyloxy radicals. This simple model is displayed in Figure 7 for TBPB dissociation. The average initial energy of the benzoyloxy radicals may be determined by statistical means by taking into account the available

excess energy after photodissociation of the parent peroxide (see above); the energy distribution is assumed to be Boltzmann-like with vibrational temperatures of the benzoyloxy radical of 1170 K (TBPB dissociation) and 1120 K (DBPO dissociation). Figure 7 shows the thermal distribution at 1170 K for TBPB dissociation and the energy of the $^2A_1$ state (grey horizontal line). The shaded area represents benzoyloxy radicals, which are sufficiently high in energy to exceed the barrier for direct dissociation via the $^2A_1$ state. With an energy of approximately 13 000 $cm^{-1}$ for vertical excitation into the $^2A_1$ state (as determined from our ab initio calculations), we estimate the branching ratio between the excited-state reaction and the reaction from the ground state to be 60:40 (TBPB dissociation) and 50:50 (DBPO dissociation).

These values are considered to be upper limits for the contribution of excited-state decarboxylation because energy relaxation may result in a nonnegligible cooling of intermediate radicals within the first 500 fs.

IR measurements of the initial energy of $CO_2$ formed in the decomposition of TBPB and DBPO also indicate high vibrational excitation of this photoproduct.[8] Although exact initial excess energies are difficult to estimate from these IR experiments because of overlapping solvent absorptions within the first 10 to 15 ps, approximate excess energies of (10 ± 3) kcal $mol^{-1}$ for $CO_2$ formed in TBPB and DBPO dissociation[8] (after 248.5-nm excitation) can be explained by about (50 ± 25)% decarboxylation from the excited state. The thermal-energy distribution for 1230 K for the benzoyloxy radicals after the photolysis of TBPB at 248.5 nm is displayed in Figure 7 (dashed curve). Taking the difference between the energy distributions for excitation at 248.5 and 266 nm into account, the contribution of decarboxylation from the excited state is estimated from the $CO_2$ infrared data to be close to 40% at the latter wavelength. Because of lower initial excess energy with DBPO, the contribution of the excited-state channel in the decarboxylation of benzoyloxy radicals after photolysis is estimated to be slightly lower, between 30 and 40%.

The significant lowering of the average excess energy available for ground-state decarboxylation due to the depletion of the high-energy tail of the energy distribution by excited-state decarboxylation may serve as another means to estimate the branching ratio, as will be shown below. The average energy of intermediate radicals reacting on the ground-state potential energy surface may be calculated by assuming that the high-energy tail of the energy distribution is cut off because of direct dissociation via the electronically excited $^2A_1$ state. In this way, initial average energies, $E_{int}$, for the ground-state decarboxylation of benzoyloxy radicals of 10 300 $cm^{-1}$ (TBPB dissociation) and 10 100 $cm^{-1}$ (DBPO dissociation) have been estimated. These numbers will be used in the subsequent modeling of decomposition rate constants for benzoyloxy radicals after peroxide excitation at 266 nm.

The microcanonical reaction rate constant for a molecule with internal energy $E$ is [36]

$$k(E) = \frac{W^{\ddagger}(E - E_0)}{h \cdot \rho(E)} \tag{1}$$

whose $W^{\ddagger}(E - E_0)$ and $\rho(E)$ denote the number of energetically accessible transition-state energy levels and the density of reactant states at energy $E$, respectively. We use the barrier height of $E_0$ = 8.4 kcal $mol^{-1}$ from our DFT calculations with the highest basis set (Table 1) and the ground- and transition-state frequencies of benzoyloxy (from DBPO and TBPB dissociation) given in Table 2 to calculate specific rate constants $k(E)$ directly as a function of internal energy $E$ for the benzoyloxy radical.

The time evolution of the energy distribution was modeled by a master equation (or step-ladder) model:[36]

$$\frac{dn(i,t)}{dt} = \sum_j k(i,j)\, n(j,t) - \sum_j k(j,i)\, n(i,t) - k_i(E)\, n(i,t) \tag{2}$$

where $n(i, t)$ is the number of molecules at time $t$ in state $i$, and $k(j, i)$ is the rate constant for collisional-energy transfer between the radical and the solvent from state $i$ to state $j$.

The thermal time-dependent rate constant is given by averaging over the time-dependent energy distribution $f(E, t)$:

$$k(t) = \int_0^\infty f(E,t)\, k(E)\, dE \tag{3}$$

with time-dependent "decay" of the initial energy distribution

$$f(E, t=0) = \frac{\rho(E) \exp\left(-\frac{E}{k_B T}\right)}{Q_{vib}} \tag{4}$$

with $Q_{vib}$ being the molecular partition function.

Intermolecular vibrational energy transfer was globally taken into account by assuming a standard kernel for $k(j, i)$,[83] the probability of transition between energy levels $i$ and $j$, which mimics the first-order relaxation of $f(E)$ with an overall phenomenological relaxation time of 7.5 ps, corresponding to a collision frequency of $z = 1.8 \times 10^{12}$ $s^{-1}$ for collisions of benzoyloxy radicals with *n*-heptane. This value was found to be optimal for most of the applied solvents.

Accordingly, to obtain concentration versus time profiles that may be directly compared with the experimental results, normalized concentrations, $S(t)_{norm}$, were calculated using eq 5

$$S(t)_{norm} = \frac{\sum_i n(i,t)}{\sum_i n(i, t=0)} \tag{5}$$

$S(t)_{norm}$ was subsequently convoluted with the experimental cross-correlation function. For each system, only a limited number of traces at particular wavelengths were suitable for being processed and analyzed in this way.

To determine whether specific solvent effects are involved, experimental traces for benzoyloxy decay (from TBPB and DBPO dissociation) have been measured for different solvents (Figures 8 and 9). The solid lines represent the simulated traces obtained from the parameters summarized in Tables 1 and 2 and in the figure captions. Figure 8 shows traces for the benzoyloxy radical after the decomposition of TBPB (Figure 8a) and DBPO (Figure 8b) at 266 nm in solvents of different viscosities. While propylene carbonate represents a solvent of high viscosity, the viscosity of acetonitrile is lower by nearly one order of magnitude. Obviously, the decarboxylation rate seems not to be affected by solvent viscosity at all. This is not surprising because motion along the reaction coordinate mainly involves structural changes in the C(O)O part of the radical (Figure 5) that are not subject to appreciable solvent friction. Furthermore, the small fragment $CO_2$ may be expected to escape easily from the solvent cage with the solvents employed here.

No change in decarboxylation behavior is seen for TBPB and DBPO upon going from nonpolar to polar solvents. Surprisingly,

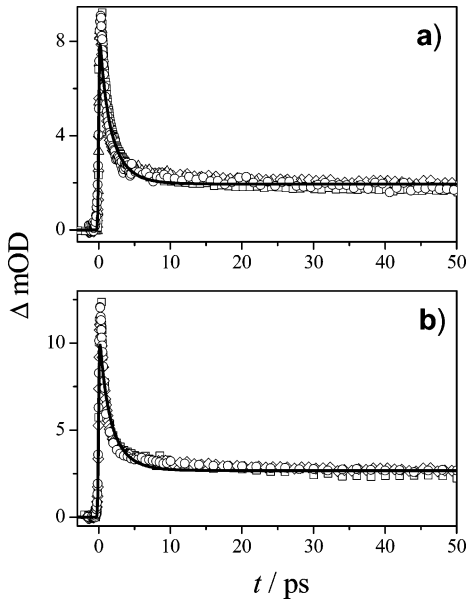


**Figure 8.** (a) Simulation of the transient absorption of benzoyloxy radicals during the photoinduced decomposition of TBPB at 266 nm in acetonitrile (◊, 700 nm), *n*-heptane (△, 700 nm), propylene carbonate (PC) (□, 594 nm), and dimethyl sulfoxide (○, 700 nm); the simulation is described in the text. Parameters: $E_{int} = 10\ 300\ cm^{-1}$, $E_0 = 8.4$ kcal $mol^{-1}$, $\tau_{vet} = 7.5$ ps. (b**)** Simulation of the transient absorption of benzoyloxy radicals during the photoinduced decomposition of DBPO at 266 nm in PC (□, 532 nm), acetonitrile (◊, 700 nm), and methanol (○, 700 nm); the simulation is described in the text. Parameters: $E_{int} = 10\ 100\ cm^{-1}$, $E_0 = 8.4$ kcal $mol^{-1}$, $\tau_{vet} = 7.5$ ps.

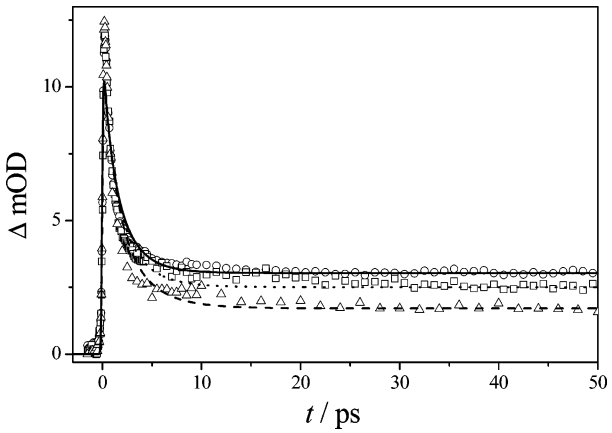


**Figure 9.** Simulation of the transient absorption of benzoyloxy radicals during the photoinduced decomposition of DBPO at 266 nm in dichloromethane (○, 700 nm), chloroform (□, 700 nm), and tetrachloromethane (△, 700 nm); lines represent simulations as described in the text. Parameters: $E_{int} = 10\ 100\ cm^{-1}$, $E_0 = 8.4$ kcal $mol^{-1}$. $\tau_{vet}$ has been chosen to be slightly different: 7 ps (—), 8 ps (···), and 10 ps (– – –).

this is also the case for DBPO even in a protic solvent such as methanol (Figure 8b). The absence of any dependence of the decarboxylation rate on the viscosity and polarity of the solvent supports our approach of predicting dissociation dynamics by a statistical model based on the energetics of the isolated molecules.

The agreement between experimental data and theoretical modeling shown in Figure 8 is very satisfactory. It is clearly seen that the rapid change starting about 300 fs after excitation corresponds to the competing processes of the fast dissociation of vibrationally hot radicals in the electronic ground states and their vibrational cooling. The apparent "offset" at longer times reflects the slow thermal decomposition at ambient temperature on a nanosecond time scale. The significant "spike" at around $t = 0$ results from a coherence artifact that is not included in the simulation.

The good agreement between theoretical modeling and experimental data can be taken as clear evidence for a significant contribution of the excited-state channel leading to lower excess energies of the benzoyloxy radicals for ground-state decarboxylation. To fit the simulated decarboxylation kinetics to the measured data under the assumption that the entire excess energy is available upon the formation of the benzoyloxy radicals without any depletion of the energy distribution via an excited-state channel, the barrier for decarboxylation needs to be 9.7 kcal $mol^{-1}$. Experimental values[48,49] and our best theoretical data (Table 1) are lower than this value by approximately 1 to 2 kcal $mol^{-1}$.

The success of our modeling with a barrier of 8.4 kcal $mol^{-1}$ (being in reasonable agreement with experimental values[48,49]) that is associated with a lower initial excess energy of the benzoyloxy radicals undergoing ground-state decarboxylation is consistent with assuming a contribution of the excited-state channel to the decarboxylation of about 20 to 50%. This percentage range is in excellent agreement with the values estimated from $CO_2$ excess energies (see above) and is corroborated by low initial yields ($\leq$ 25%) of benzoyloxy radicals found in nanosecond flash-photolysis (308 nm) studies on TBPB and DBPO decomposition.[49]

We emphasize that the simulated traces in Figure 8 were calculated from the data in Tables 1 and 2 using a global VET relaxation time of 7.5 ps. This relaxation time compares very well with experimental results for molecules[29,84] and radicals[75] of similar complexity and number of degrees of freedom. For most of the applied solvents in this study (acetonitrile, *n*-heptane, propylene carbonate, dimethyl sulfoxide, methanol, dichloromethane, and chloroform), a value between 7 and 8 ps turned out to yield the best representation of the measured decays, and for $CCl_4$, a slightly larger time constant had to be used (10 ps). These values have also been found to be optimal for describing the vibrational relaxation of structurally slightly different intermediate radicals (aryloxycarbonyloxy and benzylcarbonyloxy radicals) in these solvents.[75]

Figure 9 illustrates experiments and simulations for DBPO decomposition in three solvents. All VET times lie in the range of 7 to 10 ps. The VET time increases from dichloromethane over chloroform to $CCl_4$, which seems to be the expected trend that is also seen in other studies.[84] Nevertheless, this range of VET times is small, suggesting that no strong specific interactions between the solvent and the solute take place.

Although the agreement between curves obtained by theoretical modeling and experimental data strongly supports our model, some favorable error compensation cannot be ruled out. Further studies on organic peroxide decomposition are underway to test the general applicability of the model presented here. These data will be presented in a forthcoming publication.

## IV. Conclusions

The light-induced decarboxylation of organic peroxides in solution has been studied via absorption spectroscopy on a picosecond time scale with high (femtosecond) time resolution. In the present paper, results for two peroxides of the type [$R_1$−C(O)O−$OR_2$], with $R_1$ = phenyl and $R_2$ being either benzoyl or *tert*-butyl, have been investigated. Both peroxides are used as initiators in free-radical polymerization and have already been

extensively investigated on longer time scales and as thermally induced decompositions. Excitation at 266 nm yields benzoyloxy radicals (and *tert*-butoxy radicals in the case of $R_2$ = *tert*-butyl) as intermediates that further decompose into $CO_2$ and phenyl radicals. It is shown that both peroxides decompose in a sequential fashion with the second step being the decarboxylation of the benzoyloxy radical. The available excess energy of produced benzoyloxy radicals in the dissociation of TBPB and DBPO is sufficient to allow for direct decarboxylation via the second electronically excited state of $^2A_1$ symmetry. The contribution of excited-state (direct) decarboxylation is estimated from $CO_2$ excess energies and a lowering of the excess energy of benzoyloxy radicals for ground-state decarboxylation to be in the range of 20−50% for TBPB and DBPO dissociation. The rate for direct decarboxylation of intermediate radicals will be slightly (up to 10%) lower with DBPO than in the case of TBPB because of the lower initial excess energy in benzoyloxy radicals formed upon photolysis.

The sequential dissociation is very fast at high excess energies. Thus, peroxide decomposition may resemble a concerted process with the simultaneous breaking of two bonds in experiments with insufficient time resolution or in cases where radical scavengers are used to detect intermediate species.

A semiquantitative model for $R_1-C(O)O-OR_2$ decomposition that allows for an adequate understanding of the entire body of experimental observations is presented. With electronic energies, barrier heights, and vibrational frequencies of the benzoyloxy radical being available, the model affords for the prediction of dissociation dynamics. Within the present study, molecular parameters for (isolated) benzoyloxy species were obtained from DFT calculations.

Upon the basis of chemical intuition and experience, polymer chemists have long known that the peroxide decomposition rate and mechanism are determined by the structure and thermochemistry of the parent compounds and by the stability of the radical intermediates.[44] However, no definite structural dependence has been identified, and no qualitative, (semi-)quantitative, or even predictive model has been proposed so far. The correlation between peroxide structure and decarboxylation kinetics is the key feature of the model presented here. Ongoing investigations on various other peroxides suggest that it may be of more general applicability. With reliable molecular parameters deduced from DFT calculations, the model may be used for predictive purposes. In cases where such information is missing, it should provide at least qualitative guidance.

The modeling demonstrates that only a few quantities need to be known to estimate the photodissociation features of peroxides. In addition to the excess energy of the intermediate, the energy difference of excited states of the intermediate with respect to the associated ground state needs to be known, as should the barrier to reaction on the ground-state PES and the reaction enthalpy. These quantities control the branching ratio of prompt to delayed product formation from the intermediate and thus determine the overall kinetics.

**Acknowledgment.** We acknowledge financial support by the Deutsche Forschungsgemeinschaft within the Sonderforschungsbereich 357 ("Molekulare Mechanismen Unimolekularer Reaktionen"). We thank the Fonds der Chemischen Industrie for additional support, and we are grateful to AKZO Nobel for providing the peroxide samples. We further acknowledge experimental support by Ch. Grimm and J. Zerbs. We also enjoyed stimulating discussions about various aspects of this work with Professor J. Troe.

**Supporting Information Available:** Linear absorption spectra for *tert*-butyl peroxybenzoate (upper trace) and dibenzoyl peroxide (lower trace) between 240 and 320 nm. This material is available free of charge via the Internet at http://pubs.acs.org.

## References and Notes

(1) Zewail, A. H. *J. Phys. Chem. A* **2000**, *104*, 5660.
(2) *Femtosecond Chemistry*; Manz, J., Wöste, L. E., Eds.; VCH: New York, 1995; Vols. 1 and 2.
(3) De Schrywer, F. C.; De Feyter, S.; Schweitzer, G, *Femtochemistry*; Wiley-VCH: Weinheim, New York, 2001.
(4) King, J. C.; Zhang, J. Z.; Schwarz, B. J.; Harris, C. B. *J. Chem. Phys.* **1993**, *99*, 7595.
(5) Schroeder, J.; Troe, J. *Annu. Rev. Phys. Chem.* **1986**, *38*, 163.
(6) Aschenbrücker, J.; Buback, M.; Ernsting, N. P.; Schroeder, J.; Steegmüller, U. *Ber. Bunsen-Ges. Phys. Chem.* **1998**, *102*, 965.
(7) Aschenbrücker, J.; Buback, M.; Ernsting, N. P.; Schroeder, J.; Steegmüller, U. *J. Phys. Chem. B.* **1998**, *102*, 5552.
(8) Buback, M.; Kling, M.; Seidel, M. T.; Schott, F.-D.; Schroeder, J.; Steegmüller, U. *Z. Phys. Chem.* **2001**, *215*, 717.
(9) Hess, S.; Hippler, H.; Kühne, T.; Vöhringer, P. *J. Phys. Chem. A* **1999**, *103*, 5623.
(10) Lian, T.; Bromberg, S. E.; Asplund, M.; Yang, H.; Harris, C. B. *J. Phys. Chem.* **1996**, *100*, 11994.
(11) Schroeder, J.; Schwarzer, J.; Troe, J.; Vo$\beta$, F. *J. Chem. Phys.* **1990**, *93*, 2393.
(12) Schroeder, J.; Troe, J.; Vöhringer, P. *Z. Phys. Chem.* **1995**, *188*, 287.
(13) Payne, C. K.; Snee, P. T.; Yang, H.; Kotz, K. T.; Schafer, L.; Tilley, T. D.; Harris, C. B. *J. Am. Chem. Soc.* **2001**, *123*, 7425.
(14) Kotz, K. T.; Yang, H.; Snee, P. T.; Payne, C. K.; Harris, C. B. *J. Organomet. Chem.* **2000**, *596*, 16303.
(15) Kovalenko, S. A.; Eilers-König, N.; Senyushkina, T. A.; Ernsting, N. P. *J. Phys. Chem. A* **2001**, *105*, 4834.
(16) Kovalenko, S. A.; Schanz, R.; Farztdinov, V. M.; Henning, H.; Ernsting, N. P. *Chem. Phys. Lett.* **2001**, *323*, 312.
(17) Bakker, H. J.; Planken, P. C. M.; Langendijk, A. *Nature* **1990**, *347*, 745.
(18) Bakker, H. J.; Planken, P. C. M.; Kuipers, L.; Langendijk, A. *J. Chem. Phys.* **1990**, *94*, 1730.
(19) Charvat, A.; Assmann, J.; Abel, B.; Schwarzer, D. *J. Phys. Chem A* **2001**, *105*, 5071.
(20) Charvat, A.; Assmann, J.; Abel, B.; Schwarzer, D.; Henning, K.; Luther, K.; Troe, J. *Phys. Chem. Chem. Phys.* **2001**, *3*, 2230.
(21) Bingemann, D.; King, A.; Crim, F. F. *J. Chem. Phys.* **2000**, *113*, 5018.
(22) Bakker, H. J.; Planken, P. C. M.; Langendijk, A. *J. Chem. Phys.* **1991**, *94*, 6007.
(23) Bonn, M.; Brugmans, M. J. P.; Bakker, H. J. *Chem. Phys. Lett.* **1996**, *249*, 81.
(24) Cheatum, C. M.; Heckscher, M. M.; Bingemann, D.; Crim, F. F. *J. Chem. Phys.* **2001**, *115*, 7086.
(25) Deak, J. C.; Iwaki, L. K.; Dlott, D. D. *J. Phys. Chem. A* **1998**, *102*, 8193.
(26) Graener, H.; Lauberau, A. *Appl. Phys. B* **1982**, *29*, 213.
(27) Hartl, I.; Zinth, W. *J. Phys. Chem. A* **2000**, *104*, 4218.
(28) Kovalenko, S. A.; Schanz, R.; Henning, H.; Ernsting, N. P. *J. Chem. Phys.* **2001**, *115*, 3256.
(29) Schwarzer, D.; Troe, J.; Zerezke, M. *J. Chem. Phys.* **1997**, *107*, 8380.
(30) Hertwig, A.; Hippler, H.; Schmid, H.; Unterreiner, A.-N. *Phys. Chem. Chem. Phys.* **1999**, *1*, 5129.
(31) Kliner, D. A. V.; Alfano, J. C.; Barbara, P. F. *J. Chem. Phys.* **1993**, *98*, 5375.
(32) Wynne, K.; Galli, C.; Hochstrasser, R. M. *J. Chem. Phys.* **1994**, *100*, 4797.
(33) Schwarz, B. J.; Peteanu, L. A.; Harris, C. B. *J. Phys. Chem.* **1992**, *96*, 3591.
(34) Wei$\beta$, J.; May, V.; Ernsting, N. P.; Farztdinov, V.; Mühlpfordt, A. *Chem. Phys. Lett.* **2001**, *346*, 503.
(35) Elsaesser, T. In *Femtochemistry*; Manz, J., Woeste, L., Eds.; VCH: Weinheim, Germany, 1995; Chapter 18; pp 563−578.
(36) Baer, T.; Hase, W. L. *Unimolecular Reaction Dynamics: Theory and Experiments*; Oxford University Press: New York, 1996.
(37) Maul, C.; Gericke, K.-H. *Int. Rev. Phys. Chem.* **1997**, *16*, 1.
(38) Fujimori, K. In *Organic Peroxides*; Ando, W., Ed.; Wiley & Sons: New York, 1992; p 319.
(39) Sawaki, Y. In *Organic Peroxides*; Ando, W., Ed.; Wiley & Sons: New York, 1992; p 425.
(40) Barson, C. A.; Bevington, J. C. *J. Polym. Sci., Part A: Polym. Chem.* **1997**, *35*, 2955.

(41) Buback, M.; Sandmann, J. *Z. Phys. Chem.* **2000**, *214*, 583.
(42) Chateauneuf, J.; Lusztyk, J.; Ingold, K. U. *J. Am. Chem. Soc.* **1988**, *110*, 2877.
(43) Hashimoto, J.; Segawa, K.; Sakuragi, H. *Chem. Phys. Lett.* **1999**, *314*, 261.
(44) Wang, J.; Tateno, T.; Sakuragi, H.; Tokumaru, K. *J. Photochem. Photobiol.* **1995**, *92*, 53.
(45) Yamauchi, S.; Hirota, N.; Takahara, S.; Sakuragi, H.; Tokumaru, K. *J. Am. Chem. Soc.* **1985**, *107*, 5021.
(46) Yamauchi, S.; Hirota, N.; Takahara, S.; Misawa, H.; Sawabe, K.; Sakuragi, H.; Tokumaru, K. *J. Am. Chem. Soc.* **1989**, *111*, 4402.
(47) Tateno, T.; Sakuragi, H.; Tokumaru, K. *Chem. Lett.* **1992**, *20*, 1883.
(48) Misawa, H.; Sawabe, K.; Takahara, S.; Sakuragi, H.; Tokumaru, K. *Chem. Lett.* **1988**, *23*, 357.
(49) Chateauneuf, J.; Lusztyk, J.; Ingold, K. U. *J. Am. Chem. Soc.* **1988**, *110*, 2886.
(50) Kitamaru, A.; Sakuragi, H.; Yoshida, M.; Tokumaru, K. *Bull. Chem. Soc. Jpn.* **1980**, *53*, 1393.
(51) Falvey, D. E.; Schuster, G. B. *J. Am. Chem. Soc.* **1986**, *108*, 7419.
(52) Morlino, E. A.; Bohorquez, M. D.; Neckers, D. C.; Rodgers, A. A. J. *J. Am. Chem. Soc.* **1991**, *113*, 3599.
(53) Bockman, T. M.; Hubig, S. M.; Kochi, J. K. *J. Org. Chem.* **1997**, *62*, 2210.
(54) Assmann, J.; Charvat, A.; Kappel, C.; Schwarzer, D.; Luther, K.; Abel, B. *J. Phys. Chem. A* **2002**, 106, 5197.
(55) Assmann, J.; Benten, R. v.; Charvat, A.; Abel, B. *J. Phys. Chem. A* **2003**, *107*, 1904.
(56) Abel, B.; Assmann, J.; Buback, M.; Kling, M.; Schmatz, S.; Schroeder, J. *Angew. Chem., Int. Ed.* **2003**, *42*, 299.
(57) Perkampus, H.-H. *UV−Vis Atlas of Organic Compounds*, 2nd ed.; VCH: Weinheim, Germany, 1992.
(58) Dorer, F. H.; Johnson, S. N. *J. Phys. Chem.* **1971**, *75*, 3651.
(59) McBride, J. M.; Merrill, R. A. *J. Am. Chem. Soc.* **1980**, *102*, 1723.
(60) Korth, H. G.; Müller, W.; Lusztyk, J.; Ingold, K. U. *Angew. Chem., Int. Ed. Engl.* **1989**, *28*, 183.
(61) Korth, H. G.; Chateauneuf, J.; Lusztyk, J.; Ingold, K. U. *J. Org. Chem.* **1991**, *56*, 2405.
(62) Wallington, T. J.; Egsgaard, H.; Nielsen, O. J.; Platz, J.; Sehested, J.; Stein, T. *Chem. Phys. Lett.* **1998**, *290*, 363.
(63) Ikeda, N.; Nakashima, N.; Yoshihara, K. *J. Am. Chem. Soc.* **1985**, *107*, 3381.
(64) Kieninger, M.; Ventura, O. N.; Suhai, S. *Int. J. Quantum Chem.* **1998**, *70*, 253.
(65) Becke, A. D. *J. Chem. Phys.* **1993**, *98*, 5648.
(66) Lee, C.; Wang, W.; Parr, R. G. *Phys. Rev. B* **1988**, *37*, 785.
(67) Frisch, M. J.; Trucks, G. W.; Schlegel, H. B.; Scuseria, G. E.; Robb, M. A.; Cheeseman, J. R.; Zakrzewski, V. G.; Montgomery, J. A., Jr.; Stratmann, R. E.; Burant, J. C.; Dapprich, S.; Millam, J. M.; Daniels, A. D.; Kudin, K. N.; Strain, M. C.; Farkas, O.; Tomasi, J.; Barone, V.; Cossi, M.; Cammi, R.; Mennucci, B.; Pomelli, C.; Adamo, C.; Clifford, S.; Ochterski, J.; Petersson, G. A.; Ayala, P. Y.; Cui, Q.; Morokuma, K.; Malick, D. K.; Rabuck, A. D.; Raghavachari, K.; Foresman, J. B.; Cioslowski, J.; Ortiz, J. V.; Stefanov, B. B.; Liu, G.; Liashenko, A.; Piskorz, P.; Komaromi, I.; Gomperts, R.; Martin, R. L.; Fox, D. J.; Keith, T.; Al-Laham, M. A.; Peng, C. Y.; Nanayakkara, A.; Gonzalez, C.; Challacombe, M.; Gill, P. M. W.; Johnson, B. G.; Chen, W.; Wong, M. W.; Andres, J. L.; Head-Gordon, M.; Replogle, E. S.; Pople, J. A. *Gaussian98*, revision A.9; Gaussian, Inc.: Pittsburgh, PA, 1998.
(68) Gonzales, C.; Schlegel, H. B. *J. Chem. Phys.* **1989**, *90*, 2154.
(69) Gonzales, C.; Schlegel, H. B. *J. Phys. Chem.* **1990**, *94*, 5523.
(70) Knowles, P. J.; Hampel, C.; Werner, H.-J. *J. Chem. Phys.* **1993**, *99*, 5219.
(71) Amos, R. D.; Bernhardsson, A.; Bernig, A.; Celani, P.; Cooper, D. L.; Deegan, M. J. O.; Dobbyn, A. J.; Eckert, F.; Hampel, C.; Hetzer, G.; Knowles, P. J.; Korona, T.; Lindh, R.; Lloyd, A. W.; McNicholas, S. J.; Manby, F. R.; Meyer, W.; Mura, M. E.; Nicklass, A.; Palmieri, P.; Pitzer, R.; Rauhut, G.; Schütz, M.; Schumann, U.; Stoll, H.; Stone, A. J.; Tarroni, R.; Thorsteinsson, T.; Werner, H.-J.; MOLPRO, Version 2002.1.
(72) Dunning, T. H., Jr. *J. Chem. Phys.* **1989**, *90*, 1007.
(73) Kendall, R. A.; Dunning, T. H., Jr.; Harrison, R. J. *J. Chem. Phys.* **1992**, *96*, 6796.
(74) Pacansky, J.; Brown, D. W. *J. Phys. Chem.* **1983**, *87*, 1553.
(75) Abel, B.; Assmann, J.; Buback, M.; Grimm, Ch.; Kling, M.; Schmatz, S.; Schroeder, J.; Witte, T. *J. Phys. Chem. A*, submitted for publication, 2003.
(76) Hohenberg, P.; Kohn, W. *Phys. Rev. B* **1964**, *136*, 864.
(77) Perdew, J. P.; Burke, K.; Wang, Y. *Phys. Rev. B* **1996**, *54*, 16533.
(78) Perdew, J. P. In *Electronic Structure of Solids*; Ziesche, P., Eschrig, H., Eds.; Akademie Verlag: Berlin, 1991.
(79) Jaffe, L.; Prosen, E. J.; Swarc, M. *J. Chem. Phys.* **1957**, *27*, 416.
(80) Owrutsky, J. C.; Raftery, D.; Hochstrasser, R. M. *Annu. Rev. Phys. Chem.* **1994**, *45*, 519.
(81) Stratt, R. M.; Maroncelli, M. *J. Phys. Chem.* **1996**, *100*, 12981.
(82) Scaiano, J. C.; Wubbels, G. G. *J. Am. Chem. Soc.* **1981**, *103*, 640.
(83) Lenzer, T.; Luther, K.; Reihs, K.; Symonds, A. *J. Chem. Phys.* **2000**, *112*, 4090.
(84) Elsaesser, T.; Kaiser, W. *Annu. Rev. Phys. Chem.* **1991**, *42*, 83.